Bat Bot (B2), A Biologically Inspired Flying Machine

Alireza Ramezani, Xichen Shi, Soon-Jo Chung, Seth Hutchinson

***Abstract*— It is challenging to analyze the aerial locomotion of bats because of the complicated and intricate relationship between their morphology and flight capabilities. Developing a biologically inspired bat robot would yield insight into how bats control their body attitude and position through the complex interaction of nonlinear forces (e.g., aerodynamic) and their intricate musculoskeletal mechanism. The current work introduces a biologically inspired soft robot called Bat Bot (B2). The overall system is a flapping machine with 5 Degrees of Actuation (DoA). This work reports on some of the preliminary untethered flights of B2. B2 has a nontrivial morphology and it has been designed after examining several biological bats. Key DoAs, which contribute significantly to bat flight, are picked and incorporated in B2's flight mechanism design. These DoAs are: 1) forelimb flapping motion, 2) forelimb mediolateral motion (folding and unfolding) and 3) hindlimb dorsoventral motion (upward and downward movement).**

I. INTRODUCTION

In recent years, much effort has been devoted for producing insect-size [1] and bird-size flapping robots [2]. These robots have potential applications in surveillance and rescue missions. Also, Micro Areal Vehicles (MAV) are attracting platforms for studying, developing and pushing the boundaries of flight control algorithms for systems that have nontrivial morphologies and do not fall in the category of conventional rotary wing or fixed-wing robots. In Particular, recent developments of MAVs that are biologically inspired reveal that these small flying robots can perform very agile maneuvers similar to their biological counterparts [3]. The current work pursues the recent efforts [4], [5], [6] in studying bats' array of physiological and flight specializations by employing bat-inspired robots.

From an engineering standpoint, how difficult is it to reverse-engineer bat flight? Bats have the most sophisticated powered flight mechanism among animals. This flight mechanism has several types of joints (e.g., ball-and-socket joints, revolute joints), which interlock the bones and muscles to one another and create a metamorphic musculoskeletal system that has over 40 Degrees of Freedom (DoF), some of which are passive while some are active [7]. This articulated mechanism possesses speed-dependent morphing properties [8], [9].

It is very challenging to replicate the adaptive properties of the bat flight mechanism. In general, one wingbeat cycle consists of two movements. First, a downstroke movement is initiated by both left and right forelimbs expanding backwards and sideways while sweeping downward and forward relative to the body. Second, an upstroke movement brings the forelimbs upward and backward and is followed by flexion of the elbows and wrists to fold the wings. The bat flight mechanism yields several different moving patterns at different aerial locomotion speeds. At very slow flight speeds (for example, those that approach hovering), the forelimb downstroke motion brings the wings forward and ventrally, while the forelimb upstroke brings the wings backward and dorsally, creating the very well-known wingtip reversal. By employing these supination movements, bats produce thrust and lift forces even during the wing upstroke motion [10]. Bats have very articulated wings, which help them to have a very pronounced supination movement. In contrast to slow aerial locomotion, during fast flight speeds, the wings sweep dorsoventrally and roughly perpendicular relative to the body. Also, the supination disappears as the flight speed increases [11].

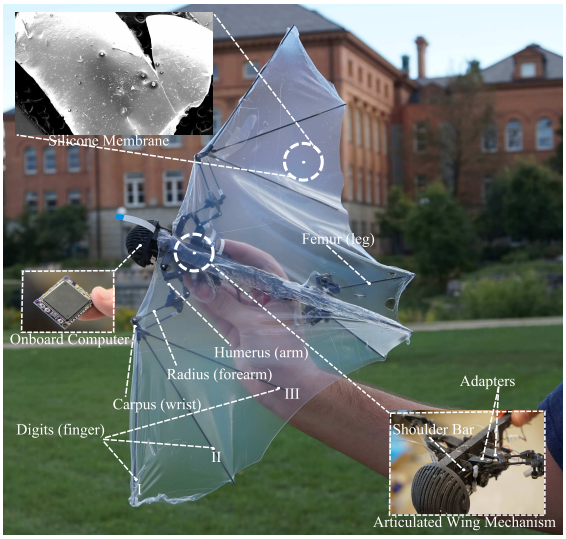

Fig. 1: UIUC bat robot, B2.

There are several challenges in developing bird-size MAVs [12], [13]. In particular, in designing a bat-inspired MAV there are several restrictions (e.g., weight, size, and power) that motivate better understanding and selection of key DoFs in bats. This yields a reduced order machine with fewer DoAs that is yet capable of mimicking its biological counterparts. A similar approach has led to successful replications of human terrestrial locomotion by employing bipedal robots that have point feet [14]. This work suggest that feet are the redundant elements of human locomotion system.

Assigning importance to the kinematic parameters of a mechanism can yield a simpler mechanism with fewer kine-

This research was supported by NSF Grant 1427111.

A. Ramezani, X. Shi, S.-J. Chung, and S. Hutchinson are with the University of Illinois at Urbana-Champaign, Urbana, IL 61801. Email:aramez,shi12,sjchung,seth@illinois.edu.

matic parameters if those parameters with higher kinematic contribution and significance are chosen. Such kinematic characterization methods have been successfully applied to study locomotion gaits in various biological mechanisms [15], [16], [17]. The work [7] employs methods based on the approach of Principle Component Analysis (PCA) in order to project bat joint movements to the subspace of Eigenmodes (EMs) and shows that by utilizing only the first EM, 34% of biological bat flight kinematics is reproducible. And, by superimposing the first and second EMs over 57% of the bat flight kinematics can be replicated.

B2 shown in Fig. 1 is designed based on biologic findings [18], [19] that emphasize the existence of functional group joints in bats. Using functional group joints makes it possible to describe the sophisticated movements of limbs during flight. There are three possible reasons why these group joints are present in bats: 1) a group of muscles has common neural stimuli, 2) the emergence of pretension forces in the membrane as it stretches passively interlocks several bones and joints to each other or 3) aerodynamic specializations in bats demands multiple joints to move in unison. In the design of B2's flight mechanism several links are physically coupled in order to synthesize a morphing structure that possesses 5 DoAs and requires minimum numbers of actuators, while at the same time is capable of producing biologically meaningful movements. The 5 DoAs include synchronous flapping motion of the left and right forelimbs (1-DoA), asynchronous mediolateral motion of the wings (2-DoA) and asynchronous dorsoventral movement of the legs (2-DoA). The morphology of B2 is nontrivial due to the presence of a custom-made silicone membrane that cannot take predefined shapes and is passively shaped by the skeletal system of B2. This introduces infinite numbers of Degrees of Underactuations (DoU) to the system and yields a challenging platform to control [20], [21], [22], [23]. In designing B2, copying bat morphology is only considered to the extent that it allows for further understanding of the flight specializations of biological bats. In other words, there has been no effort to reflect all DoFs of bats in B2 blindly, as this is not helpful and not possible from an engineering standpoint.

This paper is organized as follows. In section II, the morphological properties of B2 are given and compared with a bat species. Section III presents the design philosophy of B2's flight mechanism, which consists of forelimb and hindlimb mechanisms covered with an elastic custom-made silicone membrane. Section IV briefly reports the overall electronics that make it possible to fly autonomously. Next, dynamic modeling results are demonstrated, particularly performance of a Proportional-Derivative (PD) tail controller is demonstrated. Preliminary experimental untethered flight results are reported in section VI. Finally, this paper concludes by considering the overall project.

II. Morphometry

Aerodynamic effects such as induced lift and drag forces are the major forces acting on flapping systems. Bat-size flapping MAVs operate at the range of Reynolds numbers where theories of inviscid aerodynamics hold true with acceptable accuracy [23]. Although dealing with inviscid flows simplifies numerical wing aerodynamic analysis, it is not trivial to rely on available numerical methods during the course of the mechanical and control design. Here, initial key design elements are predicted from biological counterparts since there are already several allometric studies examining the aeromechanics of these animals [24], [11], [25].

Several biological bats were considered, but ultimately *Rousettus Aegyptiacus* was chosen as the basis of B2's morphological properties. The primary determining factor was the flight kinematic properties as opposed to the physical dimensions of bones. Of particular importance was nominal flight speed. In biological bats, flight speed affects several key wing kinematic properties, such as wingbeat frequency, stroke plane angle, wing stroke amplitude and span ratio. Other than these morphological variations, performance of flight is dependent on flight speed. This connection between flight speed and performance is explained by the Strouhal number, which simply describes oscillating flow mechanisms. It has been shown that bats operate at the Strouhal numbers 0.2 to 0.8 [10]. At small Strouhal numbers the flight speed is too large and the friction drag terms, which are proportional to the square of the flight speed, decrease the efficiency of flight drastically. Conversely, when the Strouhal number is too large, and this happens often near hovering flight, the efficiency of flight decreases. This means that the production of lift and thrust is energetically expensive for bats; this is one of the reason why back flick or tip reversal appears at low speed. Bats attempt to produce lift even during upstrokes. In determining B2's nominal flight speed, the Strouhal number is defined as $\mathrm{St} = \frac{\mathrm{fa}}{\mathrm{V}}$ where V, f and a are flight speed $(\mathrm{m\,s^{-1}})$, flapping frequency (Hz) and flapping amplitude (m), respectively. Projecting wing stroke in the frontal plane and measuring the distance between wingtip position at top and bottom of the stroke relative to the body gives the wingbeat amplitude. B2's nominal flight speed, wingbeat amplitude and frequency were designed such that the Strouhal number is 0.2.

Table I presents the morphological and kinematic properties of B2.

III. Novel Articulated Wing Mechanism

The nonlinear interaction between aerodynamic forces and the body during the course of a bat-inspired MAV flight adds to the complexity of flight dynamics and it makes it challenging to design a flight controller. Designing a bat-like MAV has challenges rooted in engineering design restrictions and flight control complexities. Often, many DoAs are constructed in the design of bio-inspired robots. This school of thinking has led to design and development of robots with many DoAs that simply cannot match their biological counterparts. Apart from performance issues that may appear from over-actuating a dynamic system, these approaches are not practical for bat-inspired MAVs because there are technical restrictions in terms of sensing and actuating many joints

TABLE I: Morphological and kinematic details of B2.

	B2	Bat[1]
flight speed, $\mathrm{m\,s^{-1}}$	4.0	4.4
aspect ratio, -	3.57	5.0
flapping frequency, Hz	10	≈ 10
flapping amplitude, $^\circ$	$\pm$ 27.5	≈ 35
mean wing span, m	0.469	0.6
mean wing area, m	0.0694	0.072
mean wing chord, m	0.14	0.12
wing load, $\mathrm{kg\,m^{-1}}$	1.328	2.22
total mass, kg	0.093	0.16
body width, m	0.02	0.035
humerus (arm) length, m	0.035	0.038
radius (forearm) length, m	0.045	0.068
digits (fingers) length, m	0.14	0.12
femur (leg) length, m	0.1	0.055

[1] *Rousettus aegyptiacus [25].*

in a robot that has tight weight and dimension restrictions. On the other hand, oversimplifying bat wing kinematics and assuming that the shape of the wings is as simple as a flat surface (similar to conventional ornithopters) underestimates the complexities of the bat flight mechanism. The resulting bio-inspired robot may not help answer how bats achieve their impressive agile aerial locomotion.

The method of this design was to pick coordinates that have major contribution in bats flight. B2's wings, which are shown in Fig. 1, are supported by five major components: 1) armwing, 2) proximial handwing, 3) distal handwing, 4) hindlimbs, and 5) body. The humerus and radius synthesize armwing and proximial handwings, whereas digits create the boundaries of the distal handwing. Actuating the forelimb with a single actuator deforms the wing membrane at the leading edge and actuation in the leg deforms the wing at the trailing edge. In actuating these boundaries, few DoAs are envisioned that are biologically meaningful.

A. Forelimb

Overview: Forelimbs in B2, shown in Fig. 2, consist of twelve links: humeral (p_0-p_7), humeral support (p_3-p_4), radial (p_3-p_5), radial support (p_6-p_7), carpal (p_5-p_6)and three digital links, which impart membranal mechanical support and morphing leverage. B2's forelimbs primarily fight against deformations and provide support for actuators upon which the elastic silicone membrane is morphed. Thus, aerodynamic forces can compensate for the robot's payload. The nature of such forces are different from other biologically inspired robots such as legged robots. Internal forces, particularly sheer or torsion forces, act on the limbs and other elements of B2. In legged systems, often consecutive impacts act on legs and are aligned with the axis of links. In B2, the aerodynamic forces are perpendicular on thin hollow carbon fiber tubes. In a biological bat, maximum forces emerge in three phases: 1) the end of the downstroke, 2) the end of the upstroke and 3) mid downstroke [26]. It is predicted that the end of the downstroke is load intensive because drastic changes occur in wings velocity direction. In addition, since the Center of Pressures (CoP), where aerodynamic forces act on wings, is located slightly behind the shoulder joints that connect wings to the body during downstroke, the aerodynamic forces acting in an upward direction at the CoP produce torques in humeral rotation direction[1]. In order to improve stress distribution, one solution is to increase the second moment of inertia. Hollow carbon fiber tubes are chosen in order to avoid structural failures due to excessive internal sheer and torsional stresses in B2's forelimbs. The distribution of the torsional forces across the forelimbs' links cross section are proportional to the external torque and inversely proportional to the second moment of inertia of hollow carbon fiber tubes' circular cross section.

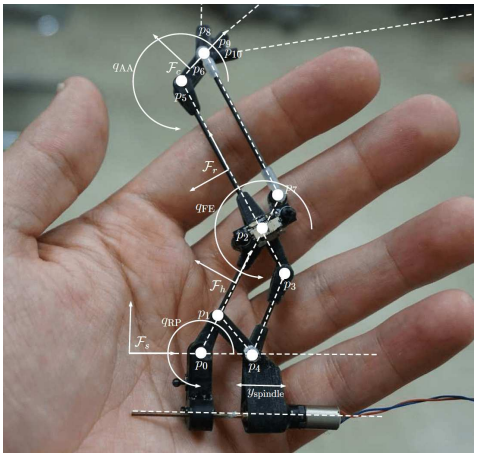

Fig. 2: B2's forelimb.

Turning to the forelimb DoFs, three functional groups, which work in unison, simply describe sophisticated wing morphing patterns in bats: when wings spread, fingers bend; when wrists pronate, elbows bend; and the medial part of the wings is morphed with the collaboration of shoulders, hips and knees [7]. Embedding humeral rotation, pronating rotation in wrists, abduction-adduction motions in digits, and flexion-extension motions in digits all require active actuation of shoulders, wrists, and finger knuckles, respectively. Engineers at Brown University have utilized string-and-pulley-based actuating mechanisms to articulate a robotic membranous wing [6]. In this design, to avoid any installment of actuators on the robotic wing, the wing is mounted on a support where a bundle including several strings is routed through the wing's links. It is then connected to several motors incorporated in the support. This way of actuation makes it possible to realize several DoAs in the robotic wing. Yet, this method is not practical for a flying MAV because it requires beefy actuators to be installed in the ribcage.

Contrary to the robotic wing of Brown University, several mechanical constraints are employed in B2 in order to synthesize a flight mechanism with a few DoAs. A three-link mechanism where three links are connected to one another with two 1-DoF revolute joints while one link is pivoted to the ground is uniquely defined mathematically

[1]Rotation around the axis of humerus link.

using three angles or configuration variables. Regulating the position and orientation of the end-effector in the three-link mechanism implies direct control of the three revolute joints. As Fig. 3 suggests, extending the mechanism with three more rigid links (constraints) results in a six-bar linkage known as Watt mechanism, which is a 1-DoF mechanism requiring only one actuator. In Fig. 3, link 6 is fixed. Each of the forelimbs are similar to a Watt six-bar linkage mechanism and their links are hinged to one another utilizing rigid 1-DoF revolute joints. The one exception is the radial support link, which is connected to the carpal plate and humeral links using two ball-and-socket joints. The rotational movement of the humeral support link around a fixed pivot is replaced by linear movements of the link relative to the humeral shoulder joint after adding a link connecting humeral and humeral support links. A linear motion of the humeral support link at the shoulder moves radial link relative to the humeral link and results in elbow flexion-extension. While humeral and radial links move with respect to each other, a relative motion of the outer digital link with respect to the radial link is realized as the elbow flexion-extension is projected to the carpal plate through the radial support link. The ball-and-socket universal joints at two ends of the support radial link facilitate the passive movements of the carpal plate in pronating direction. In contrast to biological bats, which actively rotate their wrists, B2 possesses passive carpal rotations with respect to the radius. The digital links I, II and III are cantilevered to the carpal plate and are flexible slender carbon fiber tubes that can passively flex and extend with respect to the carpal plate, meaning that they introduce 3 DoUs. In addition to the passive flexion-extension movements, the digital links can passively abduct and adduct with respect to each other resulting in extra 3 DoUs. The fingers have no knuckles and their relative angle with respect to one another is predefined. As a result, each of B2's forelimbs has 1 DoA and 6 DoU that transform linear motion of its actuator into three active and biologically meaningful movements: 1) active humeral retraction-protraction (shoulder angle), 2) active elbow flexion-extension (elbow angle) and 3) active carpal abduction-adduction (wrist angle). The passive motions include digital abduction-adduction and flexion-extension.

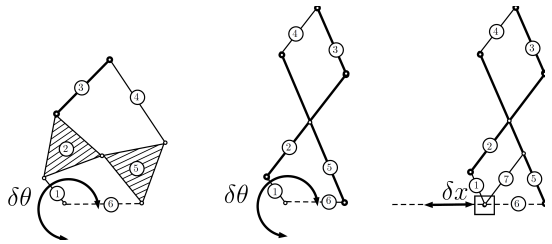

Fig. 3: Synthesis of B2's forelimb from the Watt mechanism.

Kinematic Analysis: Assuming that all of the links are rigid and all of the joints are 1-DoF revolute joints, each forelimb mechanism is uniquely defined with one configuration variable. In other words, by knowing the linear position of the spindle drive y_{spindle}, shown in Fig. 2, the configuration of the forelimbs is determined. The forelimb embodies three biologically meaningful angles. They are: the retraction-protraction angle q_{RP}, which is measured with respect to the body x-axis; the radial flexion-extension angle with respect to the humeral link q_{FE}; the abduction-adduction angle of the carpus relative to the radial link q_{AA}. The angles read positive when rotating counterclockwise. The position of each point on the forelimb mechanism is given by

$$\begin{cases} [p_i]_{\mathcal{F}_\text{s}} = [p_0]_{\mathcal{F}_\text{s}} + \mathcal{R}(q_{\text{RP}}).[p_i]_{\mathcal{F}_\text{h}}, \quad i \in \{1,2,7\} \\ [p_i]_{\mathcal{F}_\text{s}} = [p_2]_{\mathcal{F}_\text{s}} + \mathcal{R}(q_{\text{RP}}+q_{\text{FE}}).[p_i]_{\mathcal{F}_\text{r}}, \quad i \in \{3,5\} \\ [p_i]_{\mathcal{F}_\text{s}} = [p_5]_{\mathcal{F}_\text{s}} + \mathcal{R}(q_{\text{RP}}+q_{\text{FE}}+q_{\text{AA}}).[p_i]_{\mathcal{F}_\text{c}}, \\ \qquad\qquad i \in \{6,8,9,10\} \\ [p_4]_{\mathcal{F}_\text{s}} = (0, y_{\text{spindle}}, 0)^\intercal \end{cases} \tag{1}$$

where $\mathcal{F}_\text{s}$, $\mathcal{F}_\text{h}$, $\mathcal{F}_\text{r}$ and $\mathcal{F}_\text{c}$ are body coordinate frames attached to the shoulder, humerus, radius and carpus. $\mathcal{R}(q_\text{i})$ is the rotation matrix:

$$\mathcal{R}(q_\text{i}) = \begin{bmatrix} \cos(q_\text{i}) & -\sin(q_\text{i}) \\ \sin(q_\text{i}) & \cos(q_\text{i}) \end{bmatrix}. \tag{2}$$

And, $[p_i]_j$ is the position of i-th point in the body coordinate frame j. Now, the sliding constraint, which is introduced by the linear motion of the spindle drive, is incorporated into the wing kinematic equations by

$$\begin{aligned} \textbf{const}: \mathbf{G}(q_{\text{RP}}, q_{\text{FE}}, q_{\text{AA}}, y_{\text{spindle}}) = [p_4]_{\mathcal{F}_\text{s}} - \\ [p_1]_{\mathcal{F}_\text{s}} - \mathcal{R}(q_{\text{RP}}+q_{\text{FE}}).[p_4]_{\mathcal{F}_\text{r}}. \end{aligned} \tag{3}$$

Solving the nonlinear equations given by (1) subject to the constraint $\mathbf{G}(q_{\text{RP}}, q_{\text{FE}}, q_{\text{AA}}, y_{\text{spindle}})$ yields the trajectories of the forelimb links and joints (see Figs. 4 and 5).

Forelimb Actuation: An actuator, which is composed of a planetary gearhead, a spindle drive and a DC motor, produces the required linear motion, shown in Fig. 2. The actuator is mounted on the humeral support link and it weighs less than 2 g. The planetary gearhead increases the output torque and the threaded rod, which is attached to the gearhead on one side and screwed to the shoulder on the other side, pushes or pulls the shoulder depending on the direction of rotation of the spindle. At the nominal operating condition the DC motor produces angular velocity 3401 $\text{rad}\,\text{s}^{-1}$, which is geared down to 136 $\text{rad}\,\text{s}^{-1}$ utilizing the planetary gearhead. The resulting linear motion of the spindle measures 10 $\text{cm}\,\text{s}^{-1}$, which yields fast mediolateral movements of the wings. A magnetic hall effect sensor at the elbow measures the relative movements of the humeral link with respect to the radial link.

The humeral and humeral support links are hinged to the shoulder through two adapters. These adapters, shown in Fig. 1, on one side are hinged to the shoulder bar and on the other side they are pivoted to the humeral and humeral support links. This mechanism yields 1-DoF flapping motion around the shoulder bar and 1-DoF retraction-protraction motion of the humeral link. The flapping motion is realized utilizing a crank-shaft mechanism. A brushless DC motor, after it is geared down using a combination of spur compound gears embedded inside the fuselage, drives a crank

where an eccentrically attached flapping rod translates the rotary motion to push-pulls of the contact joint on the wing. The flapping mechanism synchronously produces flapping motions in right and left wings.

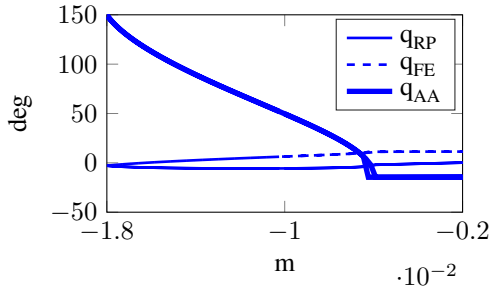

Fig. 4: Evolution of q_{RP} (shoulder), q_{FE} (elbow) and q_{AA} (wrist) versus the spindle drive position.

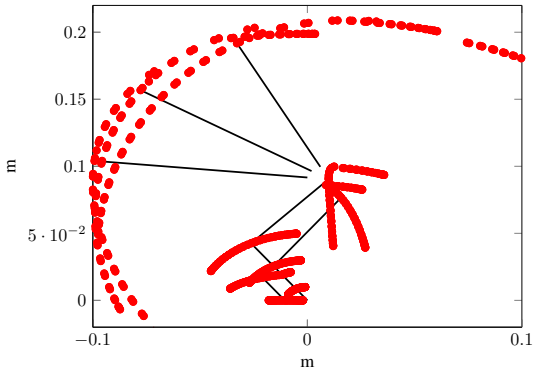

Fig. 5: Spatial evolution of the forelimb joints.

B. Hindlimb

Overview: The anatomical evolutions in bat hindlimbs enable these mammals to actively employ their hindlimbs during flight [27]. In contrast to terrestrial mammals, the ball-and-socket joint that connects the femoral bone to body is rotated in such a way that knee flexion moves the ankle ventrally [27]. The basal condition in bats yields pronounced knee flexions ventrally, which could be employed to boost flight control performance by increasing lift force, and lift-to-drag ratio, while decreasing the pitch moment. From a kinematics standpoint, the sophisticated movements of ankles in bats include dorsoventral and mediolateral movements. Ankles move ventrally during the downstroke and they start moving dorsally during the upstroke [27]. The pronounced dorsoventral movements suggest that bats actively regulate the angle of attack. But, predicting the aerodynamic consequences of hindlimb movements and determining the influence of the hindlimbs on the produced aerodynamic lift and drag forces is challenging because the movements of hindlimbs affect the membrane locally at the trailing edge of the wings, while at distal positions wings are mostly influenced by forelimbs and leg influence is negligible.

B2's legs measure 0.1 m each in length and are made out of carbon fiber rods. Each leg is hinged to the body by

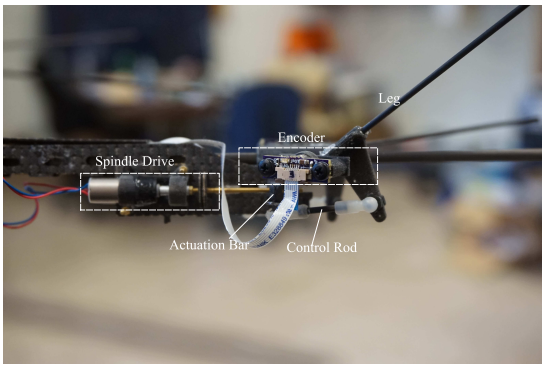

Fig. 6: Hindlimb's three-bar linkage.

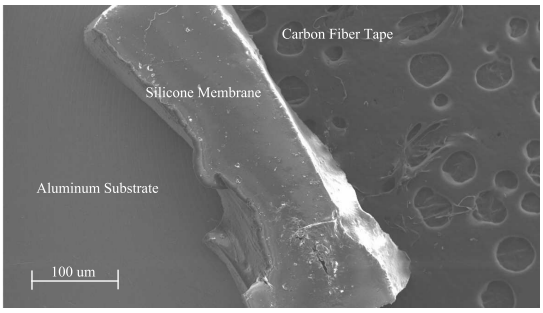

(a)

Fig. 7: Scanning Electron Microscope (SEM) image reveals that the membrane thickness is approximately 100 μm.

1-DoF revolute joints such that the produced dorsoventral movements sweep in a plane that is tilted at 30° relative to the parasagittal plane. Contrary to biological bats, B2's legs have no mediolateral movements, as such movements are less pronounced in biological bats. A three-bar linkage mechanism, which is shown in Fig. 6, composed of the leg, an actuation bar and a control rod yields the rotary movements of the legs from the linear movements of the actuation bar.

Hindlimb Actuation: As depicted in Fig. 6, a lead-screw drive similar to the forelimb spindle drive yields linear movements of the actuation bar as the threaded rod travels inside a threaded hole in the actuation bar. When the actuation bar is at its far ends, legs measure dorsoventral angles ± 30° relative to the body. A hall effect encoder reads the relative angle of the leg with respect to the body.

C. Silicone Membrane

In general, bat skin spans the body such that it is anchored to forelimbs, digital bones and hindlimbs, yielding a morphing soft mechanism that is driven by the movements of the limbs. These compliant and anisotropic structures with internal tensile forces in dorsoventral and mediolateral directions have elastin fiber bundles, which provides an extensibility and self-folding (self-packing) property to the wing membrane [28].

In producing a membranous wing for B2, after examining anatomical properties of biological skin of bats, several key

features have been considered, including weight per unit of area (area density), tensile modulus, stretchability and thickness. B2 attempts to greatly replicate these properties. A two part silicone with a platinum catalyst is pressed at or above 10,000 kg until vulcanized. It is next laser-cut to predefined shapes and attached to B2's skeleton using additional silicone. The crosslinking occurs via a platinum catalyst and silicone hydrides combined with forms of vinyl mixture. The silicone is mixed at a predefined ratio to reduce the viscosity and to ensure a thinner sheet, while giving it a greater working life. The area density is significantly important as high density membranes distributing across the robot's skeleton increase the moment of inertia of the wings along the flapping axis, and increase the overall payload of B2. Additionally, internal tensile forces introduced by the membrane to the system are of importance as the custom-made micro actuators employed in the robot have limited output performance, and when the pretension forces tops to large amounts the stall condition emerges in the actuators. This can damage the actuators as well as the power electronics. The stretchability of the produced membrane defines how viable it is for the forelimbs to retract and protract mediolaterally within their range of movements so that undesirable skin wrinkles or membrane ruptures are avoided.

The presence of the elastic membrane exposes the system to a potential field. This suggests a leverage in order to achieve energetically efficient flights. Simply speaking, at the boundaries of the membrane where forelimbs and hindlimbs meet the membrane, either the limbs and skin translate in the same directions or the opposite. These relative movements of the limbs with respect to the elastic membrane suggest that when limbs follow the membrane energy is injected to the system and when the membrane follows the limbs energy is restored in the membrane. The silicone membrane cannot push the limbs because it cannot take bending force, as the internal sheer forces deform the membrane with ease.

The elastic membrane cannot have a predefined form and is passively shaped by the skeleton upon which it is attached resulting in infinite DoUs. In other words, skin experiences passive shapes as it is deformed and cambered under B2's weight, which is supported by aerodynamic lift forces. Therefore, although the presence of the membrane suggests flight performance improvements; nevertheless, it introduces challenges from flight control standpoint.

IV. Avionics

Computing, sensing and power electronics, which are accommodated inside B2, are custom-made and yield a fully self-sustained system despite weight and size restrictions. These electronics are shown in Fig. 8. The computing unit or Main Control Board (MCB) hosts a microprocessor that has several peripherals for communication purposes. As the navigation-and-control algorithm runs on MCB in real time, a data acquisition unit acquires sensor data and commands the micro actuators. The sensing electronics, which are state-of-the-art circuit boards custom-designed in order to achieve the smallest size possible, interface the sensors and MCB by collecting two kinds of measurements. First, an Inertial Measurement Unit (IMU), which is fixed to the ribcage in such a way that x-axis points forward and z-axis points upward, reads attitudes of the robot with respect to the inertial frame. Second, four magnetic encoders are located at the elbows and hips and read the relative angles between the limbs with respect to the body. Meanwhile, the power electronics are composed of miniature MOSFETs that run several custom-made micro actuators and the brushless DC motor for flapping motion.

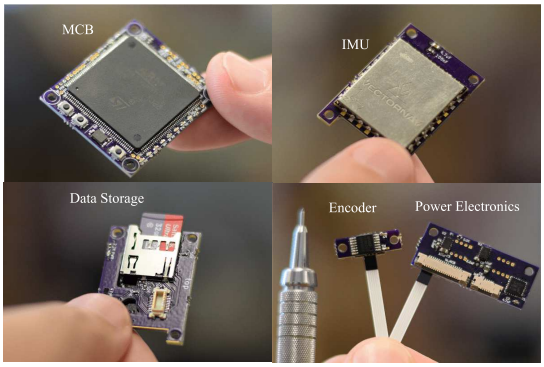

Fig. 8: B2's avionics.

V. Modeling and Closed-Loop Feedback

Flight control design for flapping systems with nontrivial morphology is challenging. Few works have made efforts to design flight controllers for bat-inspired robots applying rigorous mathematics [4], [29], [5]. In this work, a PD tail controller is designed, simulated and embedded. A more comprehensive nonlinear feedback design work for B2 is proposed in the recent work[30], which is based on variational principles and the mathematics of parametric manifolds.

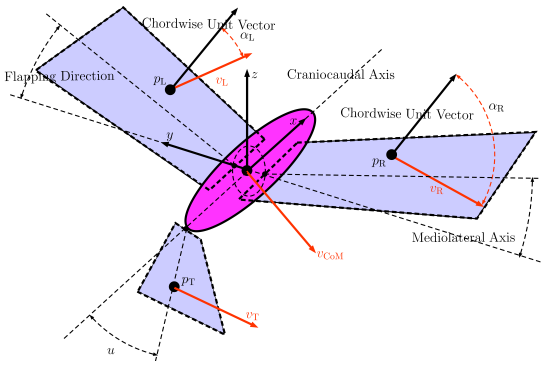

Fig. 9: B2's free-body-diagram.

The mathematical dynamic model of B2, which is depicted in Fig. 9, is developed using the Lagrange method after making the following simplifications: 1) two wings and the tail are massless, 2) the wings and the tail are separate, 3) aeroelasticity is not considered, 4) left and right wings flap synchronously and 5) both legs moves in unison with respect to the body. A Cartesian body coordinate frame

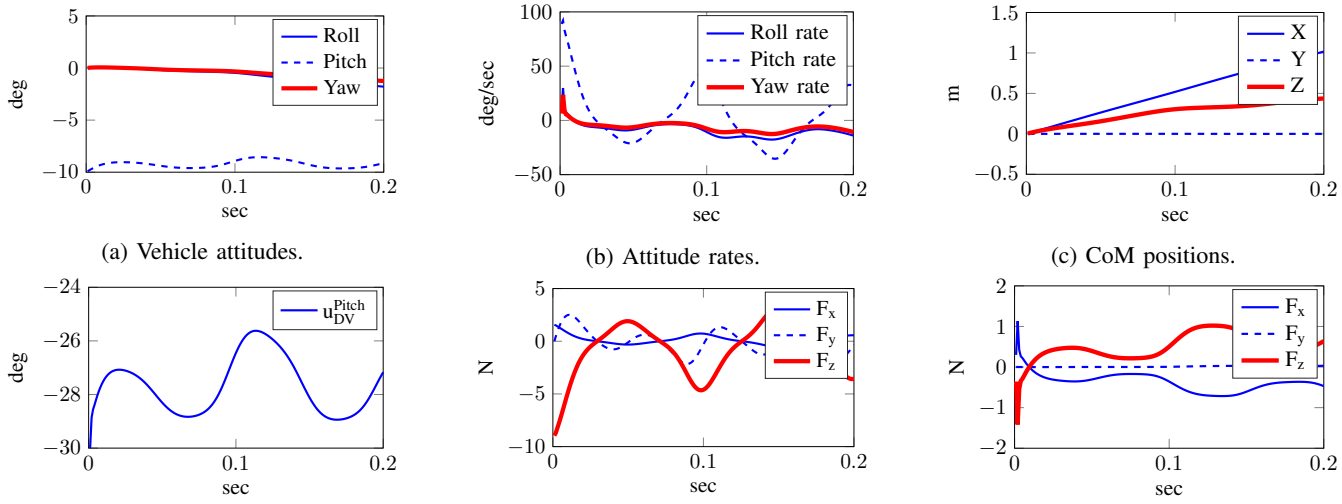

(a) Vehicle attitudes.

(b) Attitude rates.

(c) CoM positions.

(d) Control input.

(e) Aerodynamic force at left wing.

(f) Aerodynamic force at tail.

Fig. 10: Simulation results.

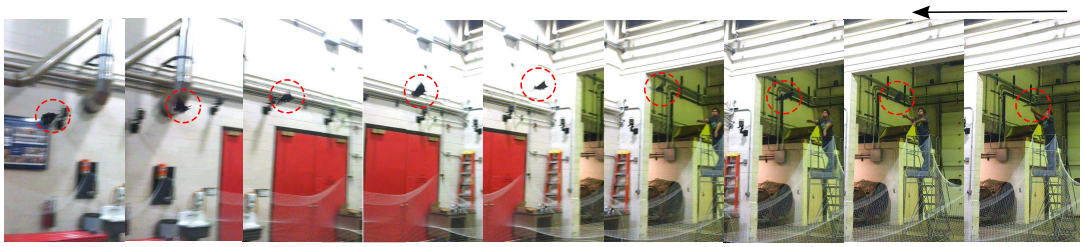

Fig. 11: Closed-loop (tail control) untethered flight.

is located at the body Center of Mass (CoM) with x-axis pointing forward and z-axis pointing upward. The configuration variable vector $\mathbf{q} \in \mathcal{Q}$ embodies q_{x}, q_{y}, q_{z}, p_{x}, p_{y} and p_{z}. Note that q_{x}, q_{y} and q_{z} are Euler-angles roll, pitch and yaw, respectively. And, p_{x} p_{y} and p_{z} are the CoM horizontal, lateral and vertical positions with respect to the inertial frame. Euler ZYX convention yields a rotation map $\mathbf{T}(q_{\mathrm{x}}, q_{\mathrm{y}}, q_{\mathrm{z}})$ from the body coordinate frame to the world inertial frame. Using the rotation matrix the attitude measurements and angular velocities are evaluated in the body coordinate frame. Applying Lagrange after evaluating the kinetic and potential energies of the body results in the following dynamics:

$$\mathcal{D}(\mathbf{q})\ddot{\mathbf{q}} + \mathcal{C}(\mathbf{q}, \dot{\mathbf{q}})\dot{\mathbf{q}} + \mathcal{G}(\mathbf{q}) = \left(\frac{\partial p_{\mathrm{L}}}{\partial \mathbf{q}}\right)^{\intercal} \mathcal{F}_{\mathrm{L}} + \left(\frac{\partial p_{\mathrm{R}}}{\partial \mathbf{q}}\right)^{\intercal} \mathcal{F}_{\mathrm{R}} + \left(\frac{\partial p_{\mathrm{T}}}{\partial \mathbf{q}}\right)^{\intercal} \mathcal{F}_{\mathrm{T}}. \tag{4}$$

where $\mathcal{D}(\mathbf{q})$, $\mathcal{C}(\mathbf{q}, \dot{\mathbf{q}})$ and $\mathcal{G}(\mathbf{q})$ capture inertia mass matrix, Coriolis, and gravity terms. In the right-hand side of (4), the generalized forces are evaluated using the principle of virtual work where p_{L}, p_{R} and p_{T} are the positions of CoP on left, right and tail wings, respectively. And, $\mathcal{F}_{\mathrm{L}}$, $\mathcal{F}_{\mathrm{R}}$ and $\mathcal{F}_{\mathrm{T}}$ are aerodynamic forces acting on left, right and tail wings. The magnitude of the aerodynamic forces are evaluated using [31]

$$\|\mathcal{F}_{\mathrm{i}}\| = \frac{3.5}{2} \rho a_{\mathrm{i}} \sin(\alpha_{\mathrm{i}}) \|v_{\mathrm{i}}\|^2, \qquad \mathrm{i} \in \{\mathrm{R}, \mathrm{L}, \mathrm{T}\} \tag{5}$$

where ρ, a_{i}, α_{i} and v_{i} are the air density, wing areas, angles of attack and CoP velocities, respectively. The aerodynamic forces act on the CoPs and they are normal to the wing cross-sections. The response of the dynamics given by (4) under the action of a feedback policy given by

$$u_{\mathrm{DV}}^{\mathrm{Pitch}} = +q_{\mathrm{y}} \kappa_{\mathrm{p}}^{\mathrm{Pitch}} + \dot{q}_{\mathrm{y}} \kappa_{\mathrm{d}}^{\mathrm{Pitch}} \tag{6}$$

is evaluated and demonstrated in Fig. 10. $u_{\mathrm{DV}}^{\mathrm{Pitch}}$ is the relative dorsoventral angle between the legs and the body. $\kappa_{\mathrm{p}}^{\mathrm{Pitch}}$ and $\kappa_{\mathrm{d}}^{\mathrm{Pitch}}$ are the controller gains.

VI. Empirical Results

The small aspect ratio and the absence of conventional control surfaces in B2 emphasize the need for a high-bandwidth closed-loop feedback policy that can compensate for attitude instability. The proposed tail controller (6) was embedded on the platform and it looped at 100 Hz while sampling the IMU and encoders at 300 Hz and 100 Hz, respectively. Untethered flight tests revealed the presence of significantly unstable rolling modes in the system mainly because of the morphological properties of B2. Therefore, the tail controller was modified by adding a roll dependent state feedback term

$$u_{\mathrm{DV}} = u_{\mathrm{DV}}^{\mathrm{Pitch}} + q_{\mathrm{x}}\kappa_{\mathrm{p}}^{\mathrm{Roll}} + \dot{q}_{\mathrm{x}}\kappa_{\mathrm{d}}^{\mathrm{Roll}} \quad (7)$$

where $\kappa_{\mathrm{p}}^{\mathrm{Roll}}$ and $\kappa_{\mathrm{d}}^{\mathrm{Roll}}$ are controller gains. Fig. 11 demonstrates the performance of B2's untethered flight as it is thrown from the top of a platform. For safety reasons, an operator has control over the throttle as there is no position feedback.

VII. Concluding Remarks

This paper presented a biologically inspired MAV called B2 in an effort to gain insight into the unrivaled agility of bat flight. The flight mechanism of B2 embodies 5 degrees of actuation: forelimb synchronous flapping, forelimb asynchronous folding and unfolding, and leg asynchronous dorsoventral movement. In addition, the presence of a custom-made silicone membrane that spans across the B2's robotic skeleton introduces several degrees of underactuation. The avionics that is embedded in B2 control the movements of joints by evaluating a navigation-and-control algorithm in real time, thereby makeing it possible to achieve autonomous self-sustained flights. This work reported B2's preliminary untethered flight using a PD-feedback policy while the forelimbs were fully stretched and the legs were the only source for the longitudinal and lateral flight control action. The synchronous actuation of the left and right legs produced stable flight in the simulation. However, due to the presence of roll unstable modes in the untethered flight tests the leg controller was modified by adding a roll state feedback. Using the feedback B2 performed an autonomous flight.

References

[1] R. J. Wood, "The first takeoff of a biologically inspired at-scale robotic insect," *Robotics, IEEE Transactions on*, vol. 24, no. 2, pp. 341–347, 2008.

[2] W. Shyy, H. Aono, S. K. Chimakurthi, P. Trizila, C.-K. Kang, C. E. Cesnik, and H. Liu, "Recent progress in flapping wing aerodynamics and aeroelasticity," *Progress in Aerospace Sciences*, vol. 46, no. 7, pp. 284–327, 2010.

[3] A. Paranjape, S.-J. Chung, J.-H. Kim *et al.*, "Novel dihedral-based control of flapping-wing aircraft with application to perching," *Robotics, IEEE Transactions on*, vol. 29, no. 5, pp. 1071–1084, 2013.

[4] S.-J. Chung and M. Dorothy, "Neurobiologically inspired control of engineered flapping flight," *Journal of Guidance, Control, and Dynamics*, vol. 33, no. 2, pp. 440–453, 2010.

[5] M. Dorothy and S.-J. Chung, "Methodological remarks on CPG-based control of flapping flight," in *AIAA Atmospheric Flight Mechanics Conference*, 2010.

[6] J. W. Bahlman, S. M. Swartz, and K. S. Breuer, "Design and characterization of a multi-articulated robotic bat wing," *Bioinspiration & biomimetics*, vol. 8, no. 1, p. 016009, 2013.

[7] D. K. Riskin, D. J. Willis, J. Iriarte-Díaz, T. L. Hedrick, M. Kostandov, J. Chen, D. H. Laidlaw, K. S. Breuer, and S. M. Swartz, "Quantifying the complexity of bat wing kinematics," *Journal of Theoretical Biology*, vol. 254, no. 3, pp. 604–615, 2008.

[8] H. Aldridge, "Kinematics and aerodynamics of the greater horseshoe bat, rhinolophus ferrumequinum, in horizontal flight at various flight speeds," *Journal of Experimental Biology*, vol. 126, no. 1, pp. 479–497, 1986.

[9] ——, "Body accelerations during the wingbeat in six bat species: the function of the upstroke in thrust generation," *Journal of Experimental Biology*, vol. 130, no. 1, pp. 275–293, 1987.

[10] A. Hedenström, L. Johansson, M. Wolf, R. Von Busse, Y. Winter, and G. Spedding, "Bat flight generates complex aerodynamic tracks," *Science*, vol. 316, no. 5826, pp. 894–897, 2007.

[11] U. M. L. Norberg and Y. Winter, "Wing beat kinematics of a nectar-feeding bat, glossophaga soricina, flying at different flight speeds and strouhal numbers," *Journal of Experimental Biology*, vol. 209, no. 19, pp. 3887–3897, 2006.

[12] D. J. Pines and F. Bohorquez, "Challenges facing future micro-air-vehicle development," *Journal of aircraft*, vol. 43, no. 2, pp. 290–305, 2006.

[13] M. F. Platzer, K. D. Jones, J. Young, and J. S. Lai, "Flapping wing aerodynamics: progress and challenges," *AIAA journal*, vol. 46, no. 9, pp. 2136–2149, 2008.

[14] C. Chevallereau, A. Gabriel, Y. Aoustin, F. Plestan, E. Westervelt, C. C. De Wit, and J. Grizzle, "Rabbit: A testbed for advanced control theory," *IEEE Control Systems Magazine*, vol. 23, no. 5, pp. 57–79, 2003.

[15] Y. P. Ivanenko, A. d'Avella, R. E. Poppele, and F. Lacquaniti, "On the origin of planar covariation of elevation angles during human locomotion," *Journal of neurophysiology*, vol. 99, no. 4, pp. 1890–1898, 2008.

[16] T. Chau, "A review of analytical techniques for gait data. part 1: fuzzy, statistical and fractal methods," *Gait & Posture*, vol. 13, no. 1, pp. 49–66, 2001.

[17] G. Cappellini, Y. P. Ivanenko, R. E. Poppele, and F. Lacquaniti, "Motor patterns in human walking and running," *Journal of neurophysiology*, vol. 95, no. 6, pp. 3426–3437, 2006.

[18] X. Tian, J. Iriarte-Diaz, K. Middleton, R. Galvao, E. Israeli, A. Roemer, A. Sullivan, A. Song, S. Swartz, and K. Breuer, "Direct measurements of the kinematics and dynamics of bat flight," *Bioinspiration & Biomimetics*, vol. 1, no. 4, p. S10, 2006.

[19] M. Rosén, G. Spedding, and A. Hedenström, "The relationship between wingbeat kinematics and vortex wake of a thrush nightingale," *Journal of Experimental Biology*, vol. 207, no. 24, pp. 4255–4268, 2004.

[20] W. Shyy, M. Berg, and D. Ljungqvist, "Flapping and flexible wings for biological and micro air vehicles," *Progress in aerospace sciences*, vol. 35, no. 5, pp. 455–505, 1999.

[21] W. Shyy, P. Ifju, and D. Viieru, "Membrane wing-based micro air vehicles," *Applied mechanics reviews*, vol. 58, no. 4, pp. 283–301, 2005.

[22] B. Stanford, P. Ifju, R. Albertani, and W. Shyy, "Fixed membrane wings for micro air vehicles: Experimental characterization, numerical modeling, and tailoring," *Progress in Aerospace Sciences*, vol. 44, no. 4, pp. 258–294, 2008.

[23] T. L. Daniel and S. A. Combes, "Flexible wings and fins: bending by inertial or fluid-dynamic forces?" *Integrative and Comparative Biology*, vol. 42, no. 5, pp. 1044–1049, 2002.

[24] F. T. Muijres, L. C. Johansson, M. S. Bowlin, Y. Winter, and A. Hedenström, "Comparing aerodynamic efficiency in birds and bats suggests better flight performance in birds," *PLoS One*, vol. 7, no. 5, pp. e37 335–e37 335, 2012.

[25] D. K. Riskin, J. Iriarte-Díaz, K. M. Middleton, K. S. Breuer, and S. M. Swartz, "The effect of body size on the wing movements of pteropodid bats, with insights into thrust and lift production," *The Journal of experimental biology*, vol. 213, no. 23, pp. 4110–4122, 2010.

[26] S. M. Swartz, M. B. Bennett, and D. R. Carrier, "Wing bone stresses in free flying bats and the evolution of skeletal design for flight," 1992.

[27] J. A. Cheney, D. Ton, N. Konow, D. K. Riskin, K. S. Breuer, and S. M. Swartz, "Hindlimb motion during steady flight of the lesser dog-faced fruit bat, cynopterus brachyotis," *PloS one*, vol. 9, no. 5, p. e98093, 2014.

[28] H. Tanaka, H. Okada, Y. Shimasue, and H. Liu, "Flexible flapping wings with self-organized microwrinkles," *Bioinspiration & biomimetics*, vol. 10, no. 4, p. 046005, 2015.

[29] S.-J. Chung, S. Bandyopadhyay, I. Chang, and F. Y. Hadaegh, "Phase synchronization control of complex networks of lagrangian systems on adaptive digraphs," *Automatica*, vol. 49, no. 5, pp. 1148–1161, 2013.

[30] A. Ramezani, X. Shi, S.-J. Chung, and S. Hutchinson, "Lagrangian modeling and flight control of articulated-winged bat robot," *Proc. 2015 IEEE/RSJ International Conference on Intelligent Robots and Systems (IROS)*, Hamburg, Germany, September 28 October 02, 2015.

[31] X. Deng, L. Schenato, and S. S. Sastry, "Flapping flight for biomimetic robotic insects: Part ii-flight control design," *IEEE Transactions on Robotics*, vol. 22, no. 4, pp. 789–803, 2006.